submitted for publication
5/26/2005

Molecular bond selective x-ray scattering for nanoscale analysis of soft matter

G. E. Mitchell,[2,*] I. Koprinarov,[1] B. G. Landes,[2] J. Lyons,[2] B. J. Kern,[2] M. J. Devon,[2] E. M. Gullikson,[3] and J. B. Kortright[3,*]

[1]*McMaster University, Hamilton, ON, Canada*

[2]*The Dow Chemical Company, Midland, MI*

[3]*Lawrence Berkeley National Lab, Berkeley, CA*

Abstract

We introduce a new technique using resonant soft x-ray scattering for characterizing heterogeneous chemical structure at nanometer length scales in polymers, biological material, and other soft matter. Resonant enhancements bring new contrast mechanisms and increased sensitivity to bridge a gap between bond-specific contrast in chemical sensitive imaging and the higher spatial resolution of traditional small-angle scattering techniques. We illustrate sensitivity to chemical bonding with the resonant scattering near the carbon K edge from latex spheres of differing chemistry and sizes. By tuning to x-ray absorption resonances associated with particular carbon-carbon or carbon-oxygen bonds we can isolate the scattering from different phases in a 2-phase mixture. We then illustrate this increased scattering contrast with a study of the templating process to form nanometer scale pores in 100 nm thick polymer films.

*To whom correspondence should be addressed. E-mail: GEMitchell@dow.com, JBKortright@lbl.gov.

For many modern polymeric materials applications, nanometer scale phase and chemical structural features determine the key macroscopic material properties. To accelerate development of such materials, tools sensitive to nanometer scale structural information as well as to the chemical composition on the same length scale are needed. Such analytical techniques need to be sensitive to both the structural relationships between different phases *and* the chemical make-up or bonding of the different phases, and thus to interrelationships between chemistry, structure, and properties. Probes of polymer structure that are currently extensively used include small-angle scattering and various microscopy techniques in which the probe particle/wave can be x-rays *(1, 2, 3*), neutrons (*4, 5*), visible or infrared light, electrons, or, in scanning probe microscopy, intermolecular forces, thermal, or magnetic properties (*6*). Small-angle scattering with hard x-rays (SAXS) or neutrons (SANS) provides ensemble-averaged information in reciprocal space whereas the microscopy techniques produce real space images of local structure.

One continuing challenge facing polymer characterization is determining heterogeneous chemical structure at the smallest spatial scale possible. Chemistry is typically resolved with various spectroscopies, such as infrared absorption (IR) or nuclear magnetic resonance (NMR) having spatial resolution of several microns or larger, respectively. Although not as chemically specific as IR or NMR, near-edge x-ray absorption fine structure spectroscopy (NEXAFS) at the carbon K edge has emerged as a powerful polymer spectroscopy because its' sensitivity to empty valence electronic orbitals provides unique fingerprints of carbon bonding in polymer and organic molecules generally (*7, 8*). NEXAFS has been combined with scanning transmission x-ray microscopy (STXM) providing analytical capability, yielding chemical sensitivity and spatial resolution down to 30 nm (*7, 9*) not available with any other microscopy technique.

Here we show that this chemical sensitivity of NEXAFS is readily extended to resonant soft x-ray scattering measurements at the carbon K edge to complement x-ray microscopy and both SAXS and SANS techniques in important ways. We demonstrate the

spectral selectivity of x-ray scattering to carbon bonding using two types of well-characterized latex spheres having different polymer phase and different sizes. We then apply this bond-sensitivity to follow processing changes in porous polymer films designed for dielectric (insulating) applications in semiconductor chips, where new insight is gained regarding the factors that control the minimum pore size in the films.

Chemical bond sensitivity is a natural consequence of resonant, or anomalous, scattering effects at atomic core levels. Anomalous scattering has been extensively used in the hard x-ray spectral range to tune the strength and phase of scattering from specific elements to resolve the phase problem in crystallography (*10*) and separate pair distribution functions in binary systems (*11*), and to enhance magnetic scattering (*12*). In the soft x-ray range resonant scattering has been used up to now in hard condensed matter to enhance magnetic (*13*) and charge (*14*) scattering, and to study charge, orbital, and spin ordering in complex oxides (*15*). While these resonant scattering effects are known to depend on the density of states near the Fermi or vacuum level, and hence on the chemical bonding of the resonant species, the natural width of hard x-ray resonances generally precludes bond-specific selectivity. By contrast, the sharp natural line widths of *soft* x-ray dipole transitions means that subtle changes in chemical bonding can clearly be resolved in resonant absorption and scattering spectra at the edges of most interest for polymer characterization (C, O and N K edges).

The sensitivity of x-ray scattering to chemically specific spectral signatures is demonstrated in Figure 1 in the C K edge absorption spectra of polystyrene (PS) and a polyacrylate (PA) copolymer of methylmethacrylate and methylacrylate. The largest peak in the PS absorption spectrum occurs at 285.2 eV and is attributable to an electronic excitation from the C 1s atomic orbital to a π^* C = C molecular orbital (*8*). The energy of this transition in PS is well below the energy at which the C K edge absorption for the acrylate polymer begins (~287 eV). The strongest absorption peak for PA occurs at 288.5 eV (C 1s $\rightarrow \pi^*$ C = O (*8*)). The energy dependence of the x-ray scattering is calculated from the absorption

spectra (*16*) for both polymers and also shown in Figure 1. The scattering spectra are similar to the absorption spectra with peaks at the same energies, but the measured scattering spectra contain refractive as well as absorptive contributions that somewhat broaden the scattering peaks relative to the absorption peaks. The effect of absorption can readily be seen by the low energy shoulder in the π* peak for the measured PA spectrum relative to the calculated spectrum in which absorption of the scattered radiation was not included. The PS spheres were small enough relative to the absorption length that the effect is unnoticeable, except, perhaps in the lower relative intensity of the π* peak in the measured spectrum. Tuning to the low energy side of strong absorption peaks can yield significantly enhanced resonant scattering for thicker samples, while avoiding the strongest absorption at the top of π* absorption peaks and minimizing radiation damage.

For the scattering experiments, the latex spheres of PS and PA were deposited, alone or mixed, onto 100 nm thick, x-ray semi-transparent, Si_3N_4 membranes (*17)* yielding sub-monolayer coverages of spheres. The spherical polymer particles have very narrow size distributions - indeed these sorts of materials are sold as size calibration standards for electron microscopy. The diameter of each monodisperse latex phase is nominally 300 nm for the PA and 79 nm for the PS. The transmission scattering geometry maintained the scattering vector $q = 4\pi\sin\theta/\lambda$ (λ is the x-ray wavelength and 2θ the scattering angle) oriented along the membrane surface. Data were collected by scanning both x-ray energy near the carbon π* resonances of these materials and θ, in each case with the other parameter fixed.

Strong bond specific resonant scattering effects are observed in energy and angle (or q) scans in both the neat and mixed phase samples. Q scans tuned to the π* peaks in the neat samples (Figure 2 a & b) yield intense patterns with multiple maxima as expected for monodisperse spherical particle ensembles (*18*). In contrast, q scans measured at the energy of scattering minima (285.6 eV for PA and 281.9 eV for PS) just below the π* peaks for each latex are 10 (PA) to 40 (PS) times less intense and show almost no indication of the classic spherical particle pattern. Energy scans for the neat samples (Figure 1 b & c) conform closely

to predictions using measured optical properties (*16*). One can, then, make use of these results in q scans of a mixture of different types of latex particles to either enhance or suppress the scattering from the different phases by appropriately adjusting the energy. For instance, by tuning near the π* peaks of the individual phases the characteristic scattering from predominantly those latex spheres is observed as seen in Figure 2c. At intermediate and remote energies the scattering contains a superposition of both contributions that is impossible to model assuming a single monodisperse latex phase. Note, however, that the resonant scattering spectra allow us to distinguish the contributions of each phase and how they vary with angle or q in the mixture (Figure 1d). Energy scans of the mixture measured near the first PS related feature (3° 2θ corresponds to q = 0.072 - 0.085 nm^{-1}) have an intense peak near 285 eV where one expects the strongest PS scattering, whereas, when an energy scan was measured at 0.8° 2θ (q = 0.019 – 0.023 nm^{-1}) there is a large peak at 288.5 eV as one expects from the neat PA scattering.

While the above measurements demonstrate that C K edge resonant scattering allows bonding and hence polymer phase identification much like NEXAFS in well-characterized samples, we turn next to less well characterized heterogeneous films having structural questions that were unresolved using previously existing techniques. These films involve two polymer phases having very similar elemental composition and densities yielding insufficient scattering contrast for SAXS measurements. Their NEXAFS spectra, however, are sufficiently different so that resonant scattering enabled measurements to analyze processing dependent structural changes in the formation of porous polymer films. Here we focus on porous polymer films for a specific application, but the new approach is relevant to a much broader class of porous polymer films produced by templating approaches, and to multiphase polymer films generally.

As feature sizes of integrated circuits shrink, it becomes important to minimize the dielectric constant (k) for the materials used as insulating films between on-chip signal paths or interconnects, to control power dissipation, limit cross-talk between signal paths and

increase device speed (*19*). One method to produce materials with lower k is to incorporate air (k = 1.0) into the film (*19*). This can be accomplished for spin-on polymer materials by a templating process in which porogen phase polymer particles are imbedded in a thermoset polymer matrix and subsequently removed after the matrix has been cured (*20*). SAXS is a well-established method to analyze pore size and loading *after* removal of the porogen (*21*). However, to understand the pore formation process, in particular to compare the resulting pore size with the original porogen size, it is essential to analyze the films with the porogen in place *before* or during processing. In the materials of interest here, porous polymers based on Dow's SiLK* family of interlayer dielectric resin based on polyphenylene (*22*), the porogen and matrix densities are nearly identical and SAXS (or even electron microscopy) provided no contrast or signal until the porogen was removed. While one can study these sorts of systems with SANS, this requires deuterating at least one of the polymer phases to provide contrast (*23*).

The carbon K NEXAFS spectra of the dense, uncured matrix and the porogen phases are seen in Figure 3a to be nearly identical. Small, subtle differences in absorption do occur in the π* resonance (the first most intense peak at 285 eV) and at about 286.5 eV. Because scattering in a porogen loaded matrix film results from the *difference* in optical properties, these subtle differences in absorption provided adequate scattering contrast and signal-to-noise. Figure 3b shows an $h\nu$ scan at a fixed $2\theta = 4^{\circ}$ ($q \cong 0.1$ nm^{-1}), which was used to determine the optimum photon energy. The strongest peak in the scattering spectrum at 284.3 eV was used for the q scans in Figure 4, and is below the π* absorption peaks both because refractive scattering contrast is strong and overall absorption of the scattered radiation is minimized at that energy.

The goal of the scattering measurements was to understand the mechanisms that limit the size and loading of pores into the final films. In this application one wants to minimize the pore size and maximize the pore loading to produce the lowest dielectric constant. Several potentially complicating issues in the templating process which could affect the size

and maximum loading of pores include swelling or agglomeration of the porogen phase in the solvent prior to introduction into the matrix, agglomeration or inadequate dispersion of the porogen in the matrix, and collapse or coalescence of resulting pores. By comparing structural attributes of the porogen particles in thin matrix films prior to their removal with the resulting pores we can gauge the importance of some of these issues.

Systematic studies investigated sets of films having three different sized porogen particles in matrices of an experimental resin. For each size, films in three processing stages were studied; as spun, after heating to 150°C to remove any trapped solvent, and after porogen removal. The two larger porogens had loadings of 20 weight percent while the smallest was added at 30% loading.

The most significant findings are seen in the comparison of the as spun films with porogen present and the end-point porous films in Figure 4. Heating to remove solvent appeared to have no effect on the porogen particle size. The results for the two larger porogens (Figs. 4a & 4b) are clearly different from those measured for the smallest porogen system (Figs. 4c). Measured q scans were fit to models based on spherical scattering centers having a Gaussian size distribution about a nominal radius of gyration R (*18*). The largest two porogens produced pores having identical size (R = 17 and 24 nm), so in these cases the porogens served as exact templates for the pore sizes in this matrix under the processing conditions used.

For the smallest porogen, however, R increased from 4 nm for the porogen to 5.8 nm for the pores. If solvent swelling of the porogen were an issue leading to the increase in pore size, it should be at least as severe with larger porogen particles and it might be expected to affect the size after the heating step. This is not observed, leaving pore collapse or coalescence during or after porogen removal as mechanisms to explain the increase in R. We can rule out agglomeration of porogen particles in the film because their size in the as-spun films determined by resonant scattering is consistent with their designed size.

Pore collapse is a function of the rigidity of the matrix – below some size limit the polymer matrix will not be rigid enough to maintain hollow pores. Coalescence of the smallest pores into larger pores to minimize surface energy is a separate but related mechanism that could account for increasing R that would also require compliance of the matrix phase, and additionally, diffusion of pores in the matrix. Comparing the dielectric properties of the processed porous films with calculations based on expected pore volume is consistent with a loss of pore volume for the smallest porogen films, supporting pore collapse in which free volume is lost to the surface, but not volume preserving coalescence. Thus we conclude that pore collapse best explains the increase in R in the smallest porogen samples, and that 5.8 nm is a reasonable experimental determination of the minimum pore size that this porogen/matrix system can support under the processing conditions used. Evidently more rigidity in the matrix is required to produce smaller pores (*24*).

This extension of scattering techniques to the carbon K edge, and other relevant absorption edges (e.g., nitrogen and oxygen) in the soft x-ray spectral range, combines several novel aspects that suggest it will become a powerful analytical tool for soft matter. Compared to SAXS, λ is ~ 10 times larger for soft x-rays so that specific structural features are found at much higher angles. This considerably eases angular resolution constraints and extends the low q limit correspondingly. Samples need not be deuterated as in SANS. Compared to soft x-ray microscopy, scattering offers higher spatial resolution because of its higher effective numerical aperture. For the porous polymer films studied here, neither SAXS, STXM at the C edge, AFM, or TEM were sensitive to the size of the porogen phase within the matrix. Only with this additional resonant sensitivity could we follow the fidelity of the porogen templating process as a function of size. Such process dependent structural information, and the understanding of nanometer scale heterogeneity generally, are increasingly important in the design of polymer and other soft matter systems. The combination of strong, sharp resonant scattering cross sections with direct sensitivity to chemical bonding yields new,

unique contrast mechanisms enabling high signal-to-noise measurements from extremely small sample volumes (*25*).

References

1. F. J. Balta-Calleja, C. G. Vonk, *X-ray Scattering of Synthetic Polymers* (Elsevier, Amsterdam, 1989).
2. O. Glatter, O. Kratky, *Small Angle X-Ray Scattering* (Academic Press, New York, 1982).
3. H. Ade, *et al*., *Science* **258**, 972 (1992).
4. R. A. Pethrick, J. V. Dawkins, Eds. *Modern Techniques for Polymer Characterization* (Wiley, New York, 1999) chap. 7.
5. D. Richter, *Physica* B **276-278**, 22 (2000).
6. V. V. Tsukruk, N. D. Spencer, Eds. *Advances in Scanning Probe Microscopy of Polymers* (Wiley–VCH, Weinheim, 2001).
7. H. Ade, S. Urquhart, in *Chemical Applications of Synchrotron Radiation*, T. K. Sham, Ed., (World Scientific, Singapore, 2002).
8. J. Stöhr, *NEXAFS Spectroscopy* (Springer-Verlag, Berlin, 1992).
9. A. L. D. Kilcoyne, *et al*., *J. Synchrotron Rad.* **10,** 125 (2003).
10. W. A. Hendrickson, *Science* **254**, 51 (1991).
11. P. H. Fuoss, P. Eisenberger, W. K. Warburton, A. Bienenstock, *Phys. Rev. Lett*. **46**, 1537 (1981).
12. D. Gibbs, *et al*., *Phys. Rev. Lett*. **61**, 1241 (1988).
13. H. Dürr, *et al*., *Science* **284**, 2166 (1999).
14. P. Abbamonte, *et al.*, *Science* **297**, 581 (2002).

15. S. B. Wilkins, *et al*., *Phys. Rev. Lett*. **90**, 187201 (2003).

16. J. B. Kortright, S.-K. Kim, *Phys. Rev. B* **62**, 12216 (2000).

17. The Si3N4 membranes were obtained from Silson Ltd, JBJ Business Park, Northampton Road, Blisworth, Northampton, NN7 3DW, England.

18. B. L. Henke, J. W. M. Dumond, *J. Appl. Phys*. **26**, 903 (1955).

19. R. D. Miller, *Science* **286**, 421 (1999).

20. R. J. Strittmatter, *et al*., in *Advanced Metallization Conference 2003,* G. W. Ray, T. Smy, T. Ohta, M. Tsujimura, Eds., (Materials Research Society, Warrendale, PA, 2004), p. 159.

21. B. Landes, *et al.*, *Mat. Res. Soc. Symp. Proc*. **766,** 209 (2003).

22. SiLK* is a trademark of The Dow Chemical Company.

23. M. S. Silverstein, *et al*., in *Characterization and Metrology for Advanced Metallization: 2003*, AIP Conf. Proc. **683** (2003).

24. Q. J. Niu, *et al*., Polymeric Materials Science and Engineering **90,** 101 (2004).

25. We acknowledge H. Ade, A. Hitchcock, and J. Kirz for their critical reading of the manuscript. Measurements were made at the Advanced Light Source at Lawrence Berkeley National Laboratory using beamlines 6.3.2 (scattering & absorption) and 7.0 (STXM & absorption). The ALS, EMG, and JBK are supported by the Director, Office of Science, Office of Basic Energy Sciences, of the U.S. Department of Energy under Contract No. DE-AC03-76SF00098.

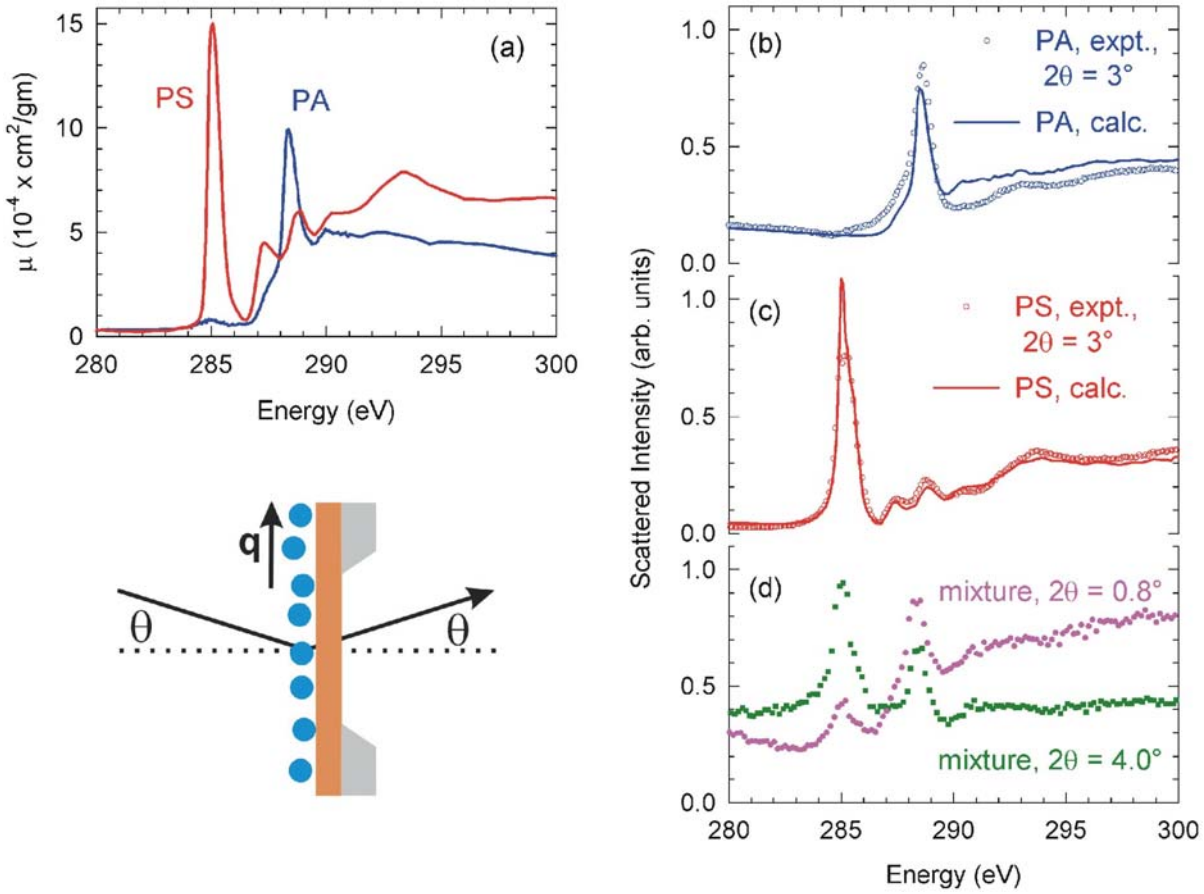

Figure 1. (a) Carbon K edge absorption spectra for PS and PA are compared. The sharp peaks are the π* resonances corresponding to transitions from the 1s atomic to π* molecular orbitals that are characteristic of predominant C = C and C = O bonding in PS and PA, respectively. At right are measured and calculated scattering spectra of ensembles of latex spheres of PA (b), PS (c) and a mixture of both (d). The resonant scattering features correspond directly to those in the absorption spectra. Calculated scattering spectra include the refractive contribution of carbon obtained from the dispersion relations as well as the contributions of other non-resonant constituents of each phase (*13*). The superposition of the PS and PA scattering spectra are evident in the mixture, with their weighting depending on angle.

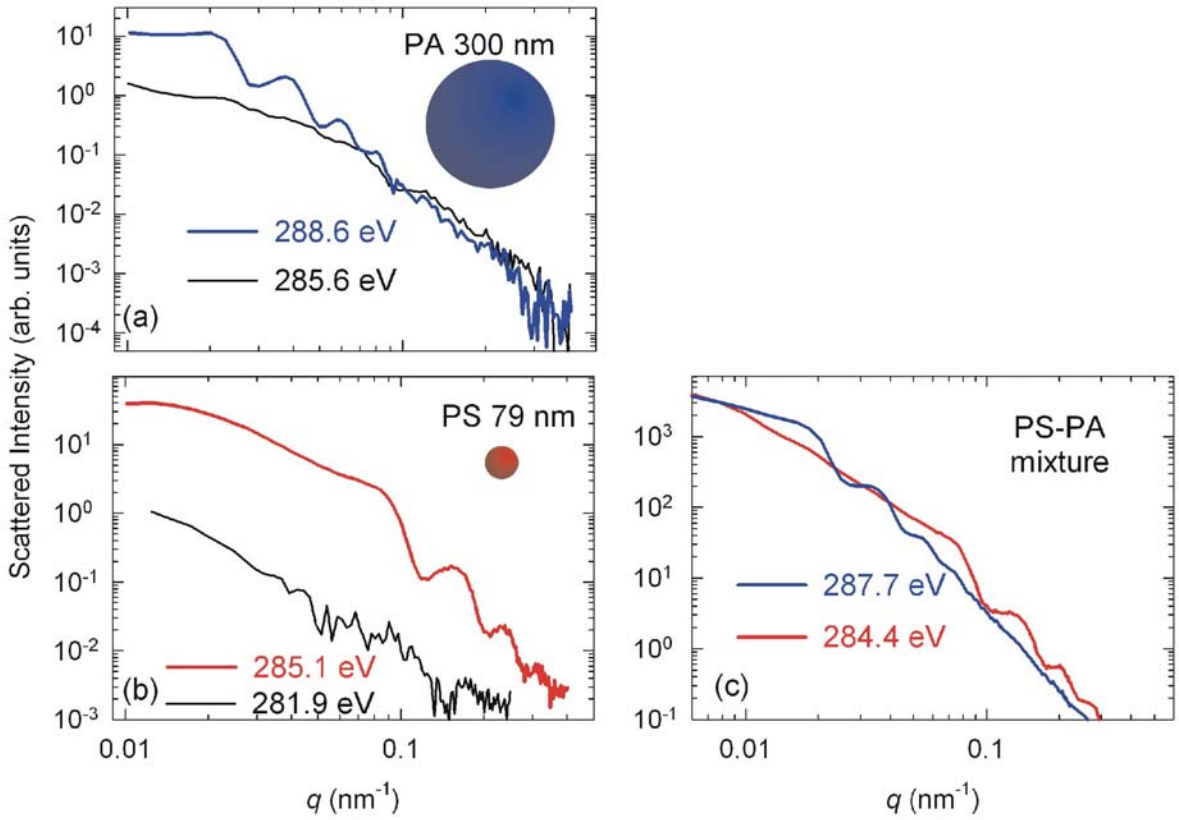

Figure 2. Normalized scattered intensity for neat assemblies of PA (a) and PS (b) latex spheres of indicated diameter show strong resonant energy dependence near the carbon K edge. When tuned to the π* line of the scattering spectra the strong, characteristic features of spherical particle scattering appear, along with some indication of interparticle interference at low q. Q scans from a mixture of PS and PA spheres (c) take the shape of either, or both, latex spheres, depending on the x-ray energy.

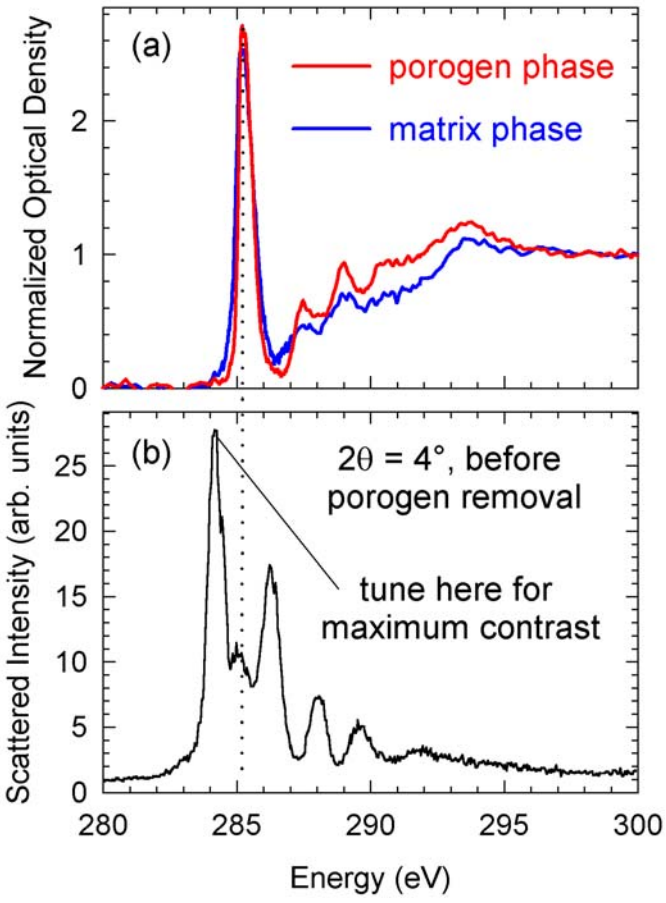

Figure 3. Two polymer phases each having significant C = C bonding have very similar absorption spectra (a). Nevertheless, a dispersion of one phase in the other exhibits strong resonant scattering contrast (b). The peaks in the scattering spectra do not fall at the same positions as the absorption peaks because of their subtle shape differences and because of absorption.

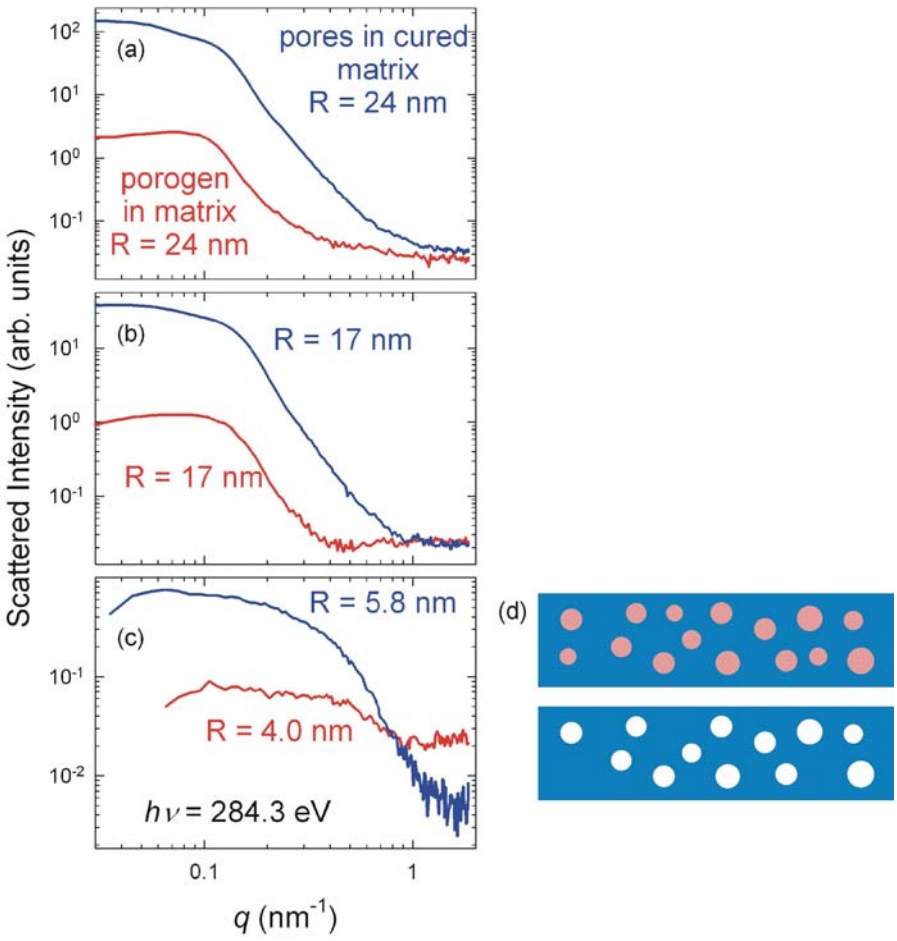

Figure 4. Resonant q scans for 3 heterogeneous polymer films involving the same porogen and matrix phases in which the average radius of the porogen particles is systematically varied. The red curves were measured with the porogen phase embedded in the matrix. The blue curves were measured after processing to remove the porogen phase leaving voided pores in the cured matrix phase. Each curve was analyzed using a spherical particle model including size dispersion yielding the average radius of gyration R indicated. High fidelity of the resulting pore sizes with the initial porogen sizes is evident for the larger porogens (a & b). For the smallest porogen (c) this templating process breaks down, with final pore sizes considerably larger than initial porogen size. Collapse of the smallest pores as in (d) accounts for this increase, where pink porogen particles (top) leave white voids (bottom).